



The effect of surface geometry on the aerodynamic behaviour of a football

M. Ward¹ · M. A. Passmore² · A. Spencer² · H. Hanson³ · T. Lucas³

Accepted: 24 February 2023 / Published online: 5 July 2023
© The Author(s) 2023

Abstract

Several studies have investigated the effect of surface features on the aerodynamic behaviour of a sphere or a football. Research on footballs typically compare real footballs with highly complex seam geometry and surface texture, making it difficult to identify which features influence the aerodynamic behaviour. This study commissioned many 3D printed footballs with regularly increasing seam length and surface texture to undertake a designed experiment to study these changes in a controlled fashion. Each ball was tested in a wind tunnel in non-spinning cases, or spinning about a vertical axis, at a range of speeds and key aerodynamic parameters were extracted from the data. Several methods were employed to characterise the *roughness* of each ball, and these roughness metrics were statistically tested for correlations with selected aerodynamic parameters. Using these relationships provides design guidance to football manufacturers to understand how modifying their surface geometry would influence the ball's aerodynamic behaviour. In general, increasing the volume of roughness of the ball, measured as the change in volume of the ball introduced through seams or texture compared to a smooth sphere, decreased the critical Reynolds number. Balls with larger texture elements, particularly those with protrusive texture, had a much lower critical Reynolds number than other balls with the same absolute volumes of roughness. The post-critical drag coefficient did not significantly correlate with any of the roughness features of the balls. In a spinning case, the balls with high roughness generated a higher side force, this relationship plateaued at a certain level of roughness. The reverse Magnus behaviour changed significantly with the surface roughness; as the overall roughness volume of the ball increased, the Reynolds number at which the reverse Magnus changed to a conventional Magnus effect decreased. The large protrusive texture elements were effective at preventing a reverse Magnus effect from occurring at all in the tested Reynolds number range.

1 Introduction

Football is the most watched and played sport in the world, with more than 3.5 billion people watching the 2018 World Cup [1], so it is important that the equipment used is satisfactory. There are standards in existence for controlling the performance of footballs with regard to circumference, sphericity, rebound, water absorption, weight, and pressure loss [2], but there are none which govern the flight behaviour of the ball. If the ball is perceived to behave abnormally, pundits, managers and players often speak [3, 4] about qualitative features of a ball flight, such as *swerve*, *dip* or *curve*; but it is unclear exactly which aspect of the flight they are referring to, how to measure them, or if they are desirable characteristics of the ball. There are no unified accepted quantifiable metrics for assessing the flight performance of a ball with literature sources [5–8] using many different methods of comparing flights, often drawing conclusions from a single example flight. This makes it difficult to determine

This article is a part of Topical Collection in Sports Engineering on Football Research, edited by Dr. Marcus Dunn, Mr. Johsan Billingham, Prof. Paul Fleming, Prof. John Eric Goff and Prof. Sam Robertson.

✉ M. A. Passmore
M.A.Passmore@lboro.ac.uk

M. Ward
m.ward2@lboro.ac.uk

- ¹ Sports Technology Institute, Loughborough University, Loughborough, UK
- ² Department of Aeronautical and Automotive Engineering, Loughborough University, Loughborough, UK
- ³ Adidas AG, Herzogenaurach, Germany

which aspects of the flight cause a certain perception of a football's aerodynamic behaviour, and, therefore, how to optimise the ball's design to control perceived behaviour. It would be preferable to statistically analyse ball performance across a large range of flights [9]. Even if the expectations of a football were well-defined, exactly how football designers should alter their ball to meet a desired behaviour is still somewhat unclear.

Prominent papers on fundamental sphere aerodynamics by Achenbach [10, 11] explores the aerodynamic behaviour of smooth and rough spheres and uses boundary layer theory to explain this behaviour. As the sphere's relative roughness (k/d) increased, the critical Reynolds number (Re_{crit}) decreased, and the post-critical drag coefficient value increased. Larger scale intrusive dimples have been found to introduce a region of recirculation, which reenergises the flow, allowing it to remain attached further round the sphere [12, 13]. Large scale protrusive pimples generate a strong hairpin vortex structure acting to reenergise the flow downstream of the element and delay the separation of the flow from the sphere surface [14, 15]. Both can cause a delayed separation and the onset of the critical regime at a lower Re than a smooth sphere, significantly affecting aerodynamic behaviour.

The Reynolds number (Re), drag coefficient (C_d) and spin coefficient (C_y) are non-dimensional quantities, which are normalised for airspeed, ball size and atmospheric effects and are defined in Eqs. 1, 2 and 3:

$$Re = \frac{\rho V_f d}{\mu} \quad (1)$$

$$C_d = \frac{2F_d}{\rho A V_f^2} \quad (2)$$

$$C_y = \frac{2F_y}{\rho A V_f^2} \quad (3)$$

Existing football aerodynamic literature [16–19] typically compare the loading of real footballs with different, complex surface features, making it difficult to discern exactly which feature is causing the changes. They demonstrate that footballs do significantly differ, even if the features causing the differences are less clear. For example, Passmore et al. [16] tested six FIFA approved footballs and found there was up to 50% change in the post-critical drag and a significant difference in Re_{crit} between the balls. They also identified a dependence of side force on the orientation of the ball and demonstrated that the panel arrangement affected these results.

Rogers [20] parametrically varied seam width and depth for a conventional truncated icosahedron pattern and found

that the wider and deeper seams had smaller Re_{crit} and slightly higher post-critical drag coefficient values, which is in line with Achenbach's findings [11]. Rogers also found adding small grooves or surface texture acted similar to global roughness. Hong et al. [21] tested the same seam design with varying surface texture elements and found that the drag curve remained consistent but noted changes in the orientation dependent side forces in non-spinning tests. Goff et al. [22] collated data from several sources and analysed the ball geometries and reported Re_{crit} to determine which of the parameters correlated most strongly to the aerodynamic performance, finding that the seam width was most important. These studies were undertaken on non-spinning balls, which simplifies the problem, but a football is almost always spinning in flight.

The Magnus effect occurs when a body is rotating, and its spin axis is not aligned with the flow direction. On the retreating side (moving in the same direction as the flow), the relative motion of the surface reduces the surface friction losses compared to the advancing side, resulting in the flow over the retreating side being faster than the advancing side. This difference in velocity will result in a pressure differential between the two sides, causing a side force. The reverse Magnus effect occurs around Re_{crit} . In this case, because of the relative velocity of the flow and surface, the flow on the retreating side becomes sub-critical, whilst the flow over the advancing side is post-critical. The difference in regime results in a later separation on the advancing side compared to the retreating side, biasing the wake towards the retreating side, resulting in an overall net force towards the advancing side. Passmore et al. [23] measured forces against orientation for a range of low spin rates and Re on real footballs. The spin dependent Magnus forces increased, and orientation dependent forces decreased with increasing spin reaching a similar magnitude at around 90 rpm. Beyond this spin rate, the Magnus forces began to dominate.

Computational fluid dynamics (CFD) models can be used to predict the aerodynamic forces acting on a football but require vast amounts of computational resource to do accurately. Pressure driven transition and boundary layer separation limits the choice of solver and requires a fine mesh near the wall to accurately model. Pasquali and Schnepf [24] used computational models to identify differences between footballs in a static case at great computational expense but were unable to develop a suitable model for a spinning case. Barber et al. [25] used commercial CFD tools to compare the aerodynamic forces of scanned geometries to wind tunnel data. Their errors in drag coefficient were up to 25% which is significant given the scale of geometric changes between the balls. It was determined that the range of balls, airspeeds and spin rates required for this investigation was more suited to an experimental analysis.

The literature discussed here highlights that comparing the aerodynamic behaviour of real footballs makes it difficult to determine exactly which of the changing features (seams or texture) causes the change in aerodynamic behaviour due to the complexity of their surface geometry and the large changes between balls. This study aimed to controllably introduce additional seams and surface texture on spheres in spinning and non-spinning conditions and examine the effect they have on the aerodynamic behaviour and develop the understanding of this relationship.

2 Methodology

2.1 Wind tunnel

The tests were undertaken in the Loughborough University large wind tunnel; a low speed, open circuit, closed jet wind tunnel with a 1.32×1.92 m working section. A schematic can be found in Fig. 1a. The tunnel can achieve a maximum velocity of 45 m/s ($Re \sim 7 \times 10^5$) and blockage ratio around 1.7% in the working section based on a ball diameter of 220 mm [26]. The balance is a high accuracy, 6-axis under-floor, virtual centre balance with a quoted component accuracy $\pm 0.05\%$ and $\pm 0.50\%$ for typical drag and side force values, respectively. A schematic of the wind tunnel inlet and test section, as well as the axis conventions used can be found in Fig. 1b. Drag is defined as positive in the positive X direction, and lateral forces are positive in the negative Y direction (such that a conventional Magnus effect results in a positive force). A 20 mm stainless steel shaft was used to support the ball from below the tunnel floor, as shown in Fig. 1c, where it was attached to a DC motor via a flexible coupling. This motor was mounted on the 6-axis force balance. All the raw data was processed using MATLAB r2021a.

To measure the drag as a function of Re of each ball, the speed was regularly increased from 10 to 30 m/s and refined around the critical speed over a non-spinning ball. 30 s of balance data was captured at 300 Hz at each point.

To measure the orientation dependency of the ball, the tunnel speed was increased from 10 to 30 m/s in steps of 5 m/s. At each speed, the ball was yawed about the Z axis through 360° in steps of 5° . Where possible, 0° was set with a seam vertical to the oncoming flow. 30 s of balance data was taken at 300 Hz at each orientation. Wind-off tare measurements were also taken and corrected for. To measure the spin dependent forces, the ball was spun from 100 to 400 rpm in steps of 100 rpm and at each spin rate the tunnel speed was set to 32 m/s and then allowed to slow down to perform a transient Reynolds sweep. The balance data was continually captured at 300 Hz as the speed decreased. This was repeated four times for each spin rate and the balance results were averaged across 1 m/s bins. This transient approach is more representative than discrete points as the ball is generally slowing down during play.

Key values were extracted from the aerodynamic data to characterise the ball's aerodynamic behaviour: the *critical Reynolds number* was manually selected from the drag data, where it plateaus from the critical into the post-critical region (defined by Achenbach [10]). The drag coefficient values for all Re above this were averaged to calculate the *post-critical drag coefficient*. The *RMS side force coefficient* was extracted from the orientation results. From the spinning tests, the *high spin side force coefficient* was defined as the side force coefficient at 200 rpm, 100 kph ($Re \sim 4.5 \times 10^5$), as well as the *minimum side force coefficient* across the range of Re at 100 rpm. The Reynolds number at which the side force became positive at 100 rpm was defined as the *reverse Magnus Reynolds number*.

2.2 Ball specifications

The balls were created using NX10.0 software (Siemens Software) starting from a smooth sphere with the required mounting features. To vary the length of seam in a controlled fashion, increasingly complex spherical polyhedra were used. These geometries were chosen to maintain a uniform distribution of seam. All the geometries used in this study can be constructed entirely from a combination of *great*

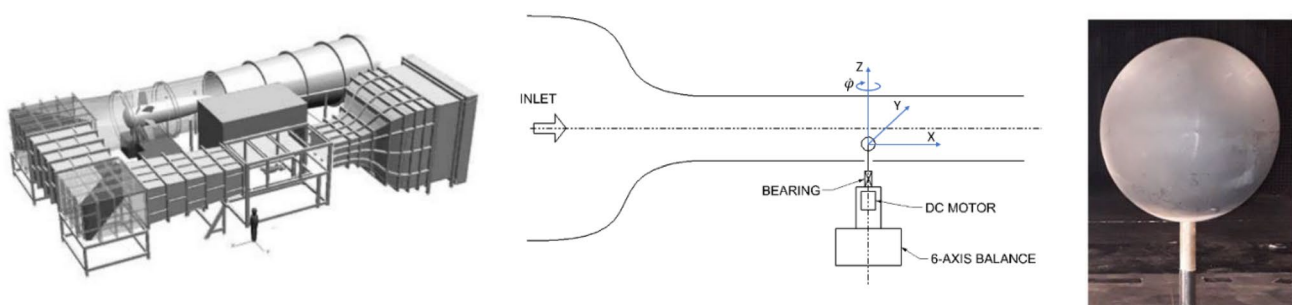


Fig. 1 a Wind tunnel schematic [27]. b Wind tunnel inlet and working section schematic, including axis conventions. c Example ball on support

circles which are circumferences of the sphere around the centre point. Key geometric properties are shown in Table 1 as well as renderings of the geometries. The seams were V-shaped, and the seam width and depth values were independently varied from 2 to 5 mm and 1 to 2.5 mm, respectively. The seam length was calculated as $2\pi R$ multiplied by the number of great circles. The specific seam dimensions for each ball are defined in Table 3.

The textures used were all spherical indentations or protrusions and are summarised in Table 2, as well as a graphical rendering. The number of elements of each texture size was selected to maintain a similar total volume of texture with each other [28] at a value consistent with a real football. The Brazuca (2014 World Cup ball) had a similar size and number of elements to the small texture; the large texture is a similar size to a golf ball dimple. The texture elements were evenly distributed over the sphere surface using a technique adapted from that described by Deserno [29]. This algorithm regularly positioned the elements, such that the

linear circumferential distance between them was the same and avoided placing them within 1 mm of a seam.

To test all five of the geometric parameters (*number of seams, seam width, seam depth, texture size, and texture direction*) in combination, an orthogonally designed experiment was followed to design the balls. This used the L16b orthogonal array design [30] and each ‘test’ was a ball design with a specific seam geometry and texture. In addition to these 16 balls, the eight balls with no seams (Table 2), as well as a smooth ball with no texture or seams were designed. The resulting ball parameter combinations are shown in Table 3. All these balls were 3D printed using a Hewlett–Packard Jet Fusion machine using a polyamide 12 material. This has a quoted layer resolution of 80 μm [31] which, whilst a similar order of magnitude to the small texture elements, was refined enough to resolve them and an order of magnitude smaller than the other features in the study. Unfortunately, two of the balls were unable to be manufactured and tested within the timeframes for this

Table 1 Seam pattern parameters

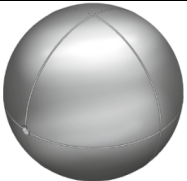



	<i>Octahedron (Oct)</i>	<i>Tetrakis Hexahedron (Hex)</i>	<i>Disdyakis Dodecahedron (Dodec)</i>	<i>Disdyakis Triacanthedron (Tric)</i>
<i>Seam Length (mm)</i>	2073	4146	6220	10367
<i>No. Edges</i>	12	36	72	180
<i>No. Great Circles</i>	3	6	9	15
<i>Rendering</i>				

Table 2 Ball texture parameters

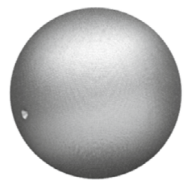
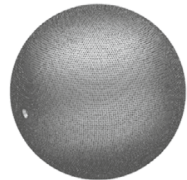
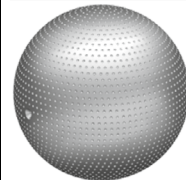
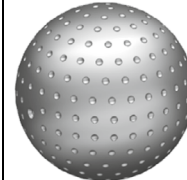
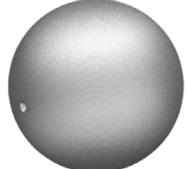
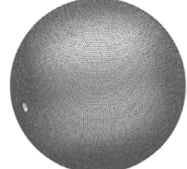
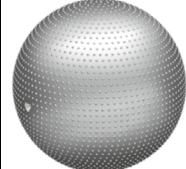
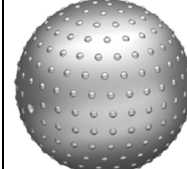
	<i>Small</i>	<i>Medium</i>	<i>Large</i>	<i>V. Large</i>
<i>Diameter (mm)</i>	1	1.4	3	8
<i>Depth (mm)</i>	0.1	0.7	1	2
<i>No. elements ($\pm 10\%$)</i>	40000	25000	3000	300
<i>Intrusive</i>				
<i>Protrusive</i>				

Table 3 Designed experiment ball specifications

	Ball #	Seam Pattern	Seam Width (mm)	Seam Depth (mm)	Texture Size	Texture Direction
L16b Orthogonal Test Matrix	1	Octahedron	2	1	None	None
	2	Octahedron	3	2.5	Med	Neg
	3	Octahedron	4	2	Large	Pos
	4	Octahedron	5	2.5	Small	Neg
	5	Hexahedron	2	1.5	Large	Neg
	6	Hexahedron	3	1	Small	Pos
	7	Hexahedron	4	2.5	None	None
	8*	Hexahedron	5	2	Med	Pos
	9	Dodecahedron	2	2	Small	Neg
	10	Dodecahedron	3	2.5	Large	Pos
	11	Dodecahedron	4	1	Med	Neg
	12	Dodecahedron	5	1.5	None	None
	13	Triacntrahedron	2	2.5	Med	Pos
	14	Triacntrahedron	3	2	None	None
	15	Triacntrahedron	4	1.5	Small	Pos
	16	Triacntrahedron	5	1	Large	Neg
Isolated Texture Balls	17	No Seam	-	-	Small	Neg
	18	No Seam	-	-	Small	Pos
	19*	No Seam	-	-	Med	Neg
	20	No Seam	-	-	Med	Pos
	21	No Seam	-	-	Large	Neg
	22	No Seam	-	-	Large	Pos
	23	No Seam	-	-	V Large	Neg
	24	No Seam	-	-	V Large	Pos
	25	No Seam	-	-	None	None

*This test programme was undertaken during the COVID-19 global pandemic which disrupted manufacture and test facility availability. The two balls marked with * were not able to be tested

investigation. This limited the formal analysis of the design of experiments results and resulted the correlation-based approach detailed in Sect. 3.4. These balls were all tested using the Reynolds sweep, yaw sweep and transient Reynolds sweep tests described in Sect. 2.1. For comparison, two real footballs, a 2014 adidas brazuca and a 2018 adidas Telstar18 were filled with expanding foam and mounted using the method detailed by Passmore et al. [5] and tested using the same method.

2.3 Equivalent roughness definition

The literature discusses the effects of various *roughness* types on the aerodynamic behaviour of a sphere. Achenbach investigates a global uniform roughness [11], Son et al. [32] apply an individual positive trip and various football literature sources [16, 18] compare different real footballs with complex seam geometry and texture. Unfortunately, it is difficult to compare these in a quantifiable way.

Footballs have three roughness types which could be considered: first, the micro-roughness of the panel material; next the individual texturing elements (dimples or pimples); and finally, the seams. Each of these are of different scales and are usually specified in different ways, so a method to characterise the overall *equivalent roughness* of the ball and to correlate this with aerodynamic behaviour is desired.

Haake et al. [33] examined cross sections of footballs and golf balls by measuring the height of each point of the ball's silhouette and statistically analysing the distribution. They found a strong relationship between Re_{crit} and skewness and that roughness dominated by valleys produced a lower Re_{crit} than roughness dominated by peaks. This analysis had only a single football geometry but worked well for golf balls. Fuss found similar trends for uniformly rough cylinders [34]. A drawback with this method is that only three planes are considered, which may be a good representation of an axisymmetric golf ball surface but less useful for a football; different results would be found if the plane chosen passes parallel to a seam, rather than perpendicular.

In this study, Haake's method was extended to consider the entire ball surface, rather than specific planes. 1 million points were evenly distributed across the surface of 3D models of the balls, using a technique defined by Deserno [29] and MATLAB r2021a to select the points and perform the analysis on the stl geometry files. At each of these points, the surface height of the computational 3D geometry was sampled and statistically analysed to produce roughness metrics. The material's micro-roughness was not considered but was an order of magnitude smaller than the seam and texture size and as the 3D printed balls used in this study were made of the same material, the micro-roughness was consistent between the balls.

Thomas [35] discusses several methods to characterise the roughness of a surface. The methods examined in this study are the mean (R_a); standard deviation (R_q); skewness (Rsk) and kurtosis (Rku). These are mathematically described in Eqs. 4, 5, 6 and 7, respectively:

$$R_a = \sum_{i=1}^N \frac{r_i}{N} \quad (4)$$

$$R_q = \sqrt{\frac{1}{N} \sum_{i=1}^N (r_i - R_a)^2} \quad (5)$$

$$R_{sk} = \frac{\sqrt{N(N-1)}}{N-2} \times \frac{\frac{1}{N} \sum_{i=1}^N (r_i - r_b)^3}{\left[\frac{1}{N} \sum_{i=1}^N (r_i - r_b)^2 \right]^{1.5}} \quad (6)$$

$$R_{ku} = \frac{N-1}{(N-2)(N-3)} \times \left[\frac{\frac{N+1}{N} \sum_{i=1}^N (r_i - r_b)^4}{\left[\frac{1}{N} \sum_{i=1}^N (r_i - r_b)^2 \right]^2} - 3(N-1) \right] \quad (7)$$

where N is the number of samples, r_i is the measured radius of each sample point, and r_b is the nominal ball radius. The skewness and kurtosis values include a correction for sample size bias (Fisher–Pearson coefficient) and the kurtosis value has been corrected, such that a perfectly normal distribution has a kurtosis of zero, not 3 [36]. The mean difference of the sample points from the mean radius was also calculated.

As well as the values used to define the 3D printed ball geometry (in Table 3) and these statistical methods, further roughness metrics were defined: *Seam length* was calculated using the number of seams and the circumference of the ball. The *seam area* was defined as the cross-sectional area of the seam. The *seam surface area* was defined as the length multiplied by the width. The *seam volume* was defined as the seam length multiplied by the

seam area. The *texture number*, *diameter* and *height* were defined in the original ball designs, and sphere–sphere intersection geometry [28] was used to determine the *texture surface area* coverage and the *texture volume* added to or removed from the sphere, described both directionally (*dir*) and absolute (*abs*), with protrusive texture being positive. The texture and seam volumes were summed to calculate the *total roughness volume*.

3 Results

3.1 Reynolds sweeps

Figure 2a shows the Reynolds sweep results for the 3D printed balls with seams but no texture elements (Balls 1, 7, 12, 15 and 25) and Fig. 2b shows the Reynolds sweep results for the 3D printed balls with texture but no seams (Balls 17–25). The effect of the support is described by Passmore et al. [16] in similar experiments. The two real footballs were also tested using the same methods and are included in Fig. 2a, these show similar critical Reynolds number and post-critical C_d results to the 3D printed balls. Adding *roughness*, either in the form of seams or surface texture, decreased Re_{crit} , the roughness acted to introduce mixing in the boundary layer and reenergise it, which is a similar finding to Achenbach [11]. The post-critical drag coefficient was reasonably consistent between all the balls, which were similar results to those found by Passmore et al. on several FIFA approved footballs [16].

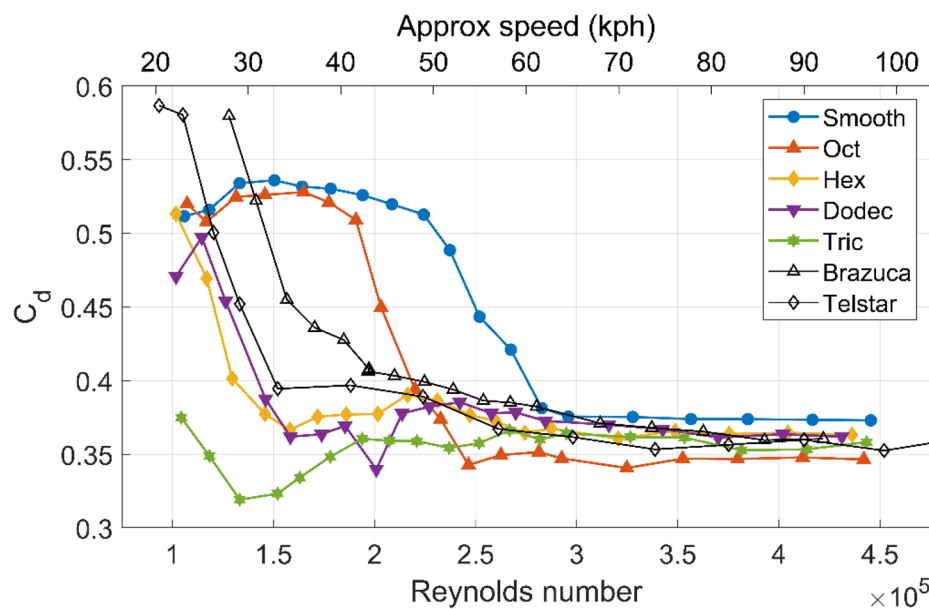
3.2 Yaw sweep results

Figure 3a shows the orientation test results for the 3D printed balls with no surface texture. Cyclic trends can be seen in the hex and dodec cases. Figure 3b shows the calculated Root-Mean-Square (RMS) side force coefficient from these results and demonstrates a clear relationship between the number of seams and the RMS side force coefficient.

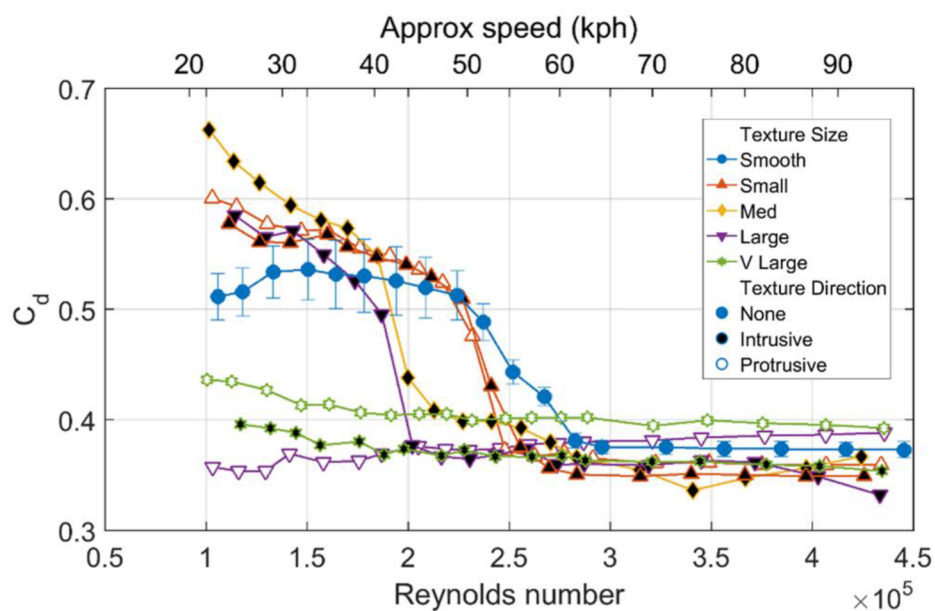
3.3 Transient Reynolds sweep test results

Figure 4 shows the side force coefficient against Re and spin rate for the 3D printed balls with no seams from the transient Reynolds sweep tests. In general, as the spin rate increased, the side force coefficient increased as the Magnus effect became stronger. The smoothest balls still exhibited a reverse Magnus effect (negative C_y) even at higher spin rates and the roughest balls never show this behaviour. The balls with some texturing show a reverse Magnus effect at low spin rates, but a conventional effect at higher spin rates.

Fig. 2 Drag coefficient against Reynolds number. **a** Effect of seams on balls with no surface texture, **b** Effect of surface texture on balls with no seams



(a)



(b)

3.4 Correlation map

The roughness and aerodynamic metrics (defined in Sect. 2) for each 3D printed ball were examined statistically using Pearson’s linear correlation methods, and the results are presented in Table 4, with R values for

significant findings ($p < 0.05$) displayed. The strongest correlations are examined in more detail in Fig. 5. Figure 5a shows that Re_{crit} decreased with increasing radius standard deviation. Figure 5b shows that as the roughness increased (either intrusive or protrusive), the side force coefficient in a spinning case increased. Figure 5c shows

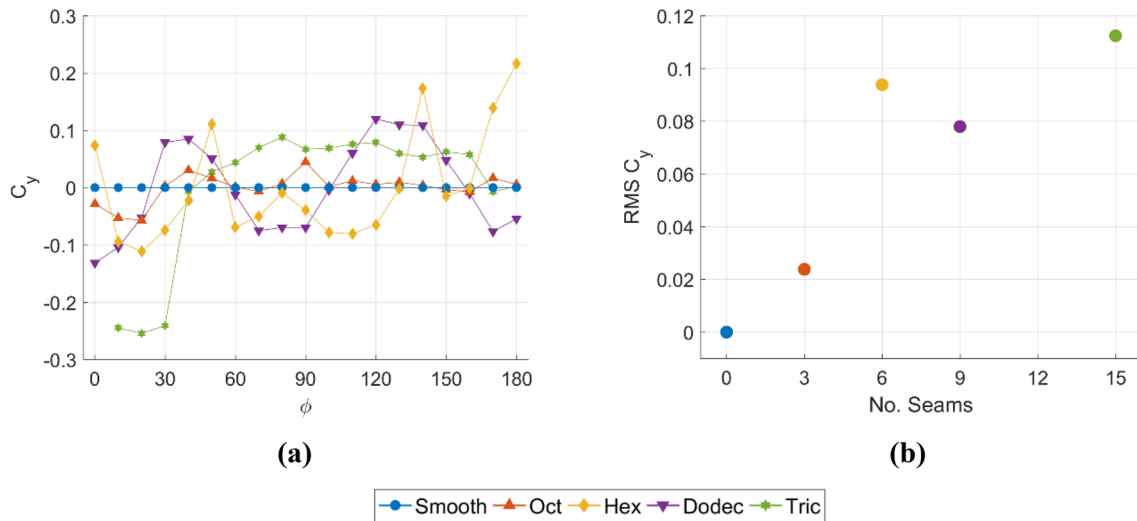


Fig. 3 Orientation test results for the balls with no surface texture. **a** side force vs orientation, **b** RMS side force coefficient

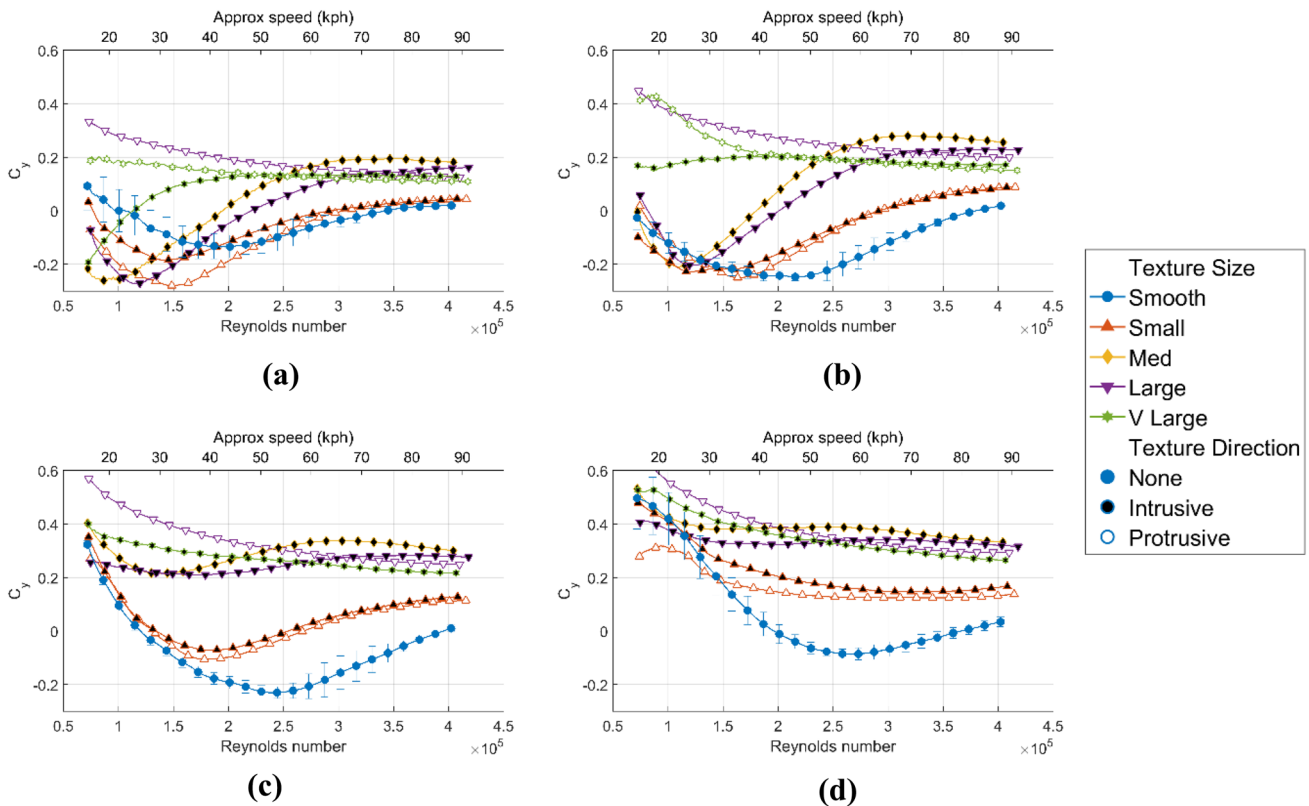


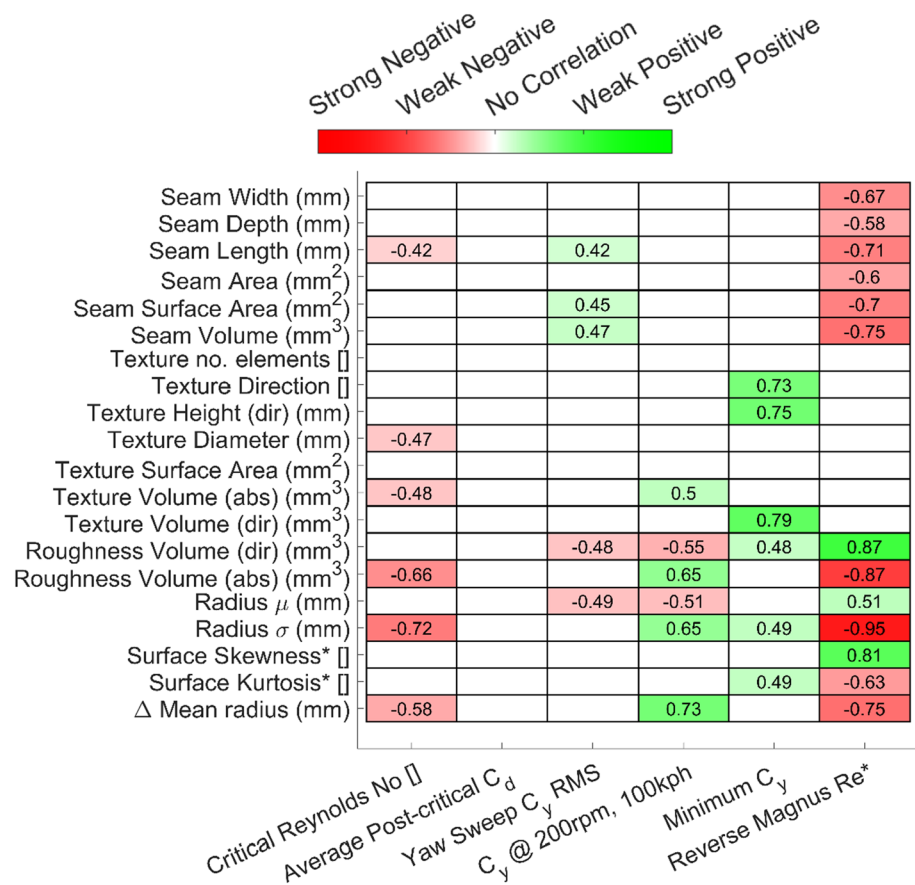
Fig. 4 Side force coefficient against Re at a range of spin rates for balls with no seam. 95% confidence intervals, representative of all cases, are only shown for the smooth ball. **a** 100 rpm, **b** 200 rpm, **c** 300 rpm, **d** 400 rpm

that as the texture volume increased the minimum side force coefficient decreased. Figure 5d shows the reverse Magnus Reynolds number decreased with an increased standard deviation.

4 Discussion

The Reynolds sweep data (Fig. 2) follows the generally

Table 4 Pearson’s linear correlation coefficients between the geometric properties and aerodynamic results



Any statistically significant relationships ($p < 0.05$) are coloured by their R value

understood phenomenon that increasing the surface roughness decreased the critical Reynolds number. Some of the most heavily textured balls did not transition at all during the range of Re tested. The orientation was not controlled in these tests, which was demonstrated by Passmore et al. to change the drag coefficient by around $\pm 5\%$. Whilst there were some small differences between the post-critical drag coefficient of the balls, the measurement repeatability and orientation effects were of this order, and as demonstrated by Passmore et al. [16] even large differences in the drag coefficient do not significantly alter the flight behaviour. The 3D printed balls were also found to match well to the results from two real footballs.

The yaw sweep results (Fig. 3) showed a strong trend that as more seams were added, the RMS side force coefficient increased. The seam dimensions also changed between the balls, an effect shown by Rogers [20] and Goff et al. [22] to be a significant contributor to the aerodynamic behaviour. The higher RMS side force coefficient for the hex ball could be because there was no equatorial seam for this geometry, meaning more of the seams on the ball had a component perpendicular to the flow, which will be more orientationally sensitive.

In the transient Reynolds sweep results (Fig. 4), the large elements decelerated the flow more significantly on the advancing side, which increased the pressure differential and hence the side force. At high Re, the side force coefficient of the larger texture elements begins to converge, but the *small* elements and smooth ball have a significantly lower side force coefficients than the others at all spin rates. There was no reverse Magnus effect seen for the protrusive *large* and *very large* textures at any spin rate or Re. In the Reynolds sweep results, it was shown that the flow regime remained post-critical throughout the range of Re tested for these balls; therefore, the laminar separation required for the reverse Magnus effect was not present. For the smaller and intrusive texture elements, there was a consistent trend that as the texture size increased, more mixing was introduced on the retreating side, which reduced the Reynolds number at which the laminar separation required for a reverse Magnus effect could occur.

The correlations found (Table 4) between Re_{crit} and increasing radius standard deviation is a similar finding to Achenbach [11], who found that uniformly increasing the ‘roughness’ caused a delayed, turbulent separation at lower Re, resulting in reduced drag. The k/d metric used by Achenbach (effectively the mean radius) did not correlate

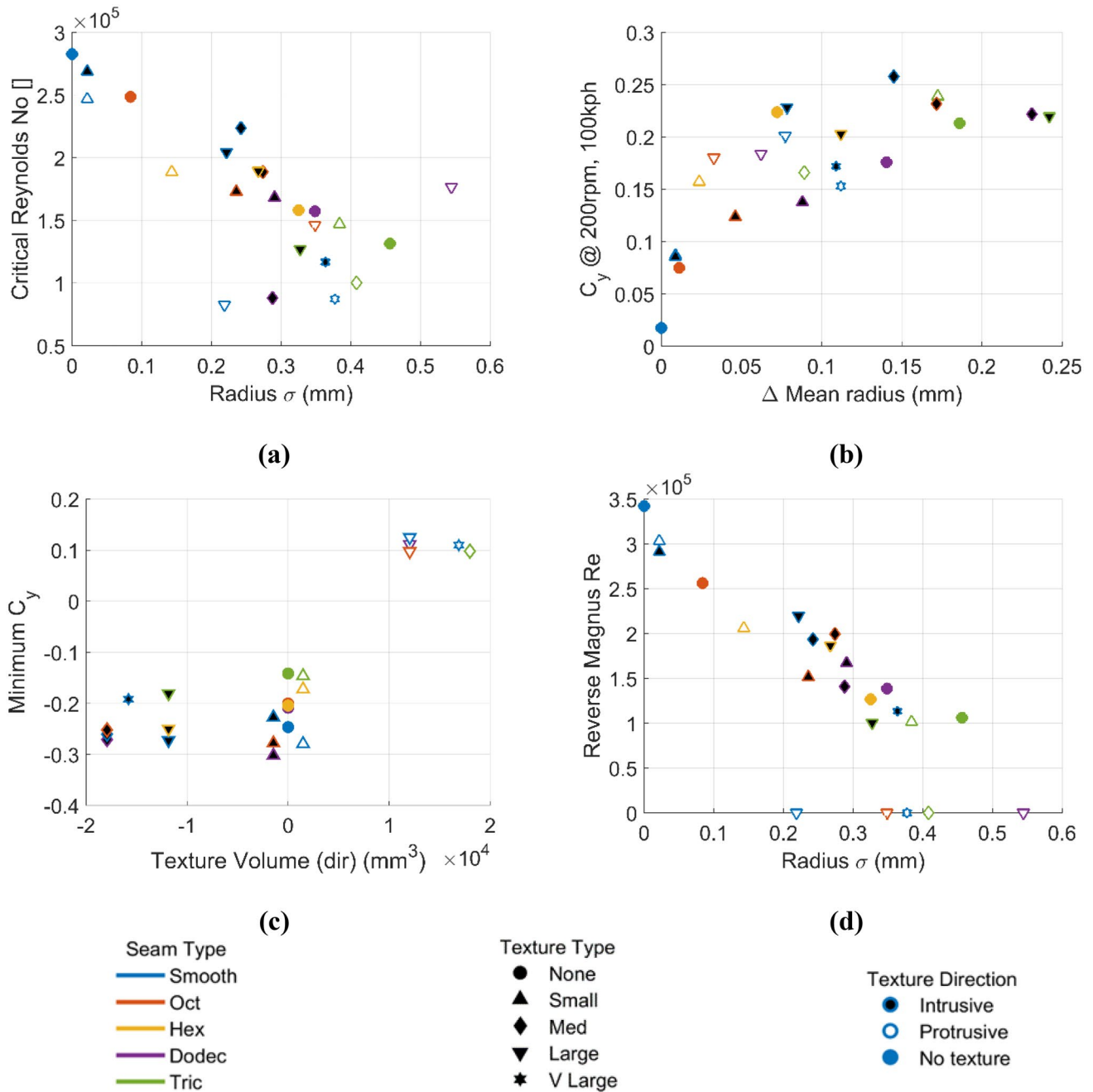


Fig. 5 Strongest correlations between roughness and aerodynamic metrics. Each marker represents one ball, the outline colour is the seam pattern, the shape is the texture size, and the fill colour represents the texture direction. **a** Re_{crit} vs surface standard deviation, **b**

side force coefficient at 200 rpm, 100kph vs absolute deviation from nominal radius, **c** minimum side force coefficient vs directional texture volume, **d** reverse magnus Re vs surface standard deviation

as strongly as these metrics as it did not effectively account for the large features, such as seams and the larger texture elements, although this relationship was still statistically significant in this analysis. Achenbach’s findings that Re_{crit} is most sensitive to the initial introduction of roughness was also in evidence here. The most significant differences from the main trend were the large protrusive textures, as well as

both intrusive and protrusive very large textures due to more effective mixing of the boundary layer. However, more typical football seam and roughness geometries were predicted well by these metrics. Goff et al. [22] found that the seam width and texture correlated best with Re_{crit} , whereas the seam length was found to correlate better in this analysis. They found that Re_{crit} decreased with increasing length and

size of seam, as was found in this study; however, they also found that Re_{crit} increased with the addition of texture, which is not consistent with Achenbach's findings [11]. As the variables in Goff et al. were not independently controlled, their finding is possibly due to the simultaneous change of seam geometry than the change in texture.

The side force increased in a spinning case with deviation from the nominal radius; the roughness on the advancing side slowed the flow down, resulting in a larger speed, and hence pressure, differential between the sides causing a larger side force. This force plateaued as the roughness increased, suggesting that the high spin side force was most sensitive to the initial roughness. The minimum side force coefficient was heavily influenced by the protrusive texture points at a very high minimum value due to their lack of reverse Magnus effect which significantly changed the appearance of the data. The large protrusive elements did not exhibit a reverse Magnus effect at any tested Re , so were given a value of zero. As the surface roughness increased, the flow on the retreating side transitioned at a lower Re , which caused the switch from reverse to conventional Magnus at a lower Re .

The 3D footballs were shown to be comparable to real footballs, but significant further investigation would be required to fully quantify the effect of the micro-roughness, and direct comparison with a similar real football would further validate this as a suitable design approach for footballs. This investigation has demonstrated empirical trends between the surface properties of a football and the aerodynamic behaviour of the ball in static and spinning conditions at a range of Reynolds numbers. There is significant further work to fully understand the fluid mechanics behind the surface and flow interaction and how these changes in flow behaviour result in the changes in measured forces. Flow measurement techniques (such as particle image velocimetry) or visualisation (such as smoke) could be useful here. One significant limitation is the presence of the support, which is known to affect the flow behaviour around the ball. Unfortunately, some element of interference is unavoidable to support the ball, and a crossflow support is necessary to enable the ball to spin. It would be an interesting further investigation to take geometric and aerodynamic measurements of real footballs to understand if these relationships hold true and further develop understanding in this area.

5 Conclusions

This study undertook a designed parametric experiment using 3D printed footballs with regularly changing surface features to identify the influence of seams and texture on the aerodynamic behaviour of the balls. Novel methods to statistically analyse the overall roughness of the ball were

developed and were tested for correlations with measured aerodynamic properties. In several cases, the metrics quantifying the combined roughness of the ball correlated better with the aerodynamic properties than any of the individual features. These relationships between the ball's surface geometry and its aerodynamic properties will allow football designers to better optimise and control their design for a desired aerodynamic performance. These relationships demonstrated that increasing the roughness of the ball, either through the introduction of seams or texture decreased Re_{crit} [6, 11, 16]. Balls with large texture elements, particularly protrusive texture, were found to be post-critical across the range of tested Re . The post-critical drag coefficient did not significantly correlate with any of the metrics of roughness of the balls. Larger seam volumes were found to have increased the orientation dependent RMS side force during the static tests. When large texture elements were added, the RMS side force reduced as the effect of the uniform texture obscured the isolated seams. In a spinning case, the smooth and smallest texture balls had much lower side force coefficients than the more heavily textured balls; this relationship plateaued at a certain level of roughness. The reverse Magnus behaviour changed significantly with the surface roughness. As the overall roughness volume of the ball increased, the Re at which the reverse Magnus changed to a conventional Magnus effect decreased with a strong linear relationship. The larger protrusive texture elements were effective at preventing a reverse Magnus effect from occurring at all in this Re range.

Funding The research leading to these results received funding from the EPSRC under Grant Agreement No. 1843979.

Declarations

Conflict of interest At the initial time of writing, the lead author received research support from adidas AG. adidas AG also kindly provided the 3D printed and real ball specimens for these experiments. M. Ward receives research support from adidas AG.

Ethical approval This manuscript is all original work by the authors or is clearly referenced.

Open Access This article is licensed under a Creative Commons Attribution 4.0 International License, which permits use, sharing, adaptation, distribution and reproduction in any medium or format, as long as you give appropriate credit to the original author(s) and the source, provide a link to the Creative Commons licence, and indicate if changes were made. The images or other third party material in this article are included in the article's Creative Commons licence, unless indicated otherwise in a credit line to the material. If material is not included in the article's Creative Commons licence and your intended use is not permitted by statutory regulation or exceeds the permitted use, you will need to obtain permission directly from the copyright holder. To view a copy of this licence, visit <http://creativecommons.org/licenses/by/4.0/>.

References

- FIFA (2018) More than half the world watched record-breaking 2018 World Cup, <https://www.fifa.com/worldcup/news/more-than-half-the-world-watched-record-breaking-2018-world-cup>. Accessed 14 April 2020
- FIFA (2017) Testing and certification for footballs, international match ball standard. Accessed 14 April 2020
- Smith J (2017) Pep Guardiola calls Mitre league cup ball ‘unacceptable’ after Wolves win. *ESPN*, <https://www.espn.co.uk/football/manchester-city/story/3242793/pep-guardiola-calls-mitre-league-cup-ball-unacceptable-after-wolves-win>. Accessed 14 April 2020
- Chandler H (2010) Controversy over new World Cup ball. *CNN*, <http://edition.cnn.com/2010/SPORT/football/06/02/football.jabulani.ball.world.cup/index.html>. Accessed 14 April 2020
- Passmore MA, Tuplin S, Spencer A et al (2008) Experimental studies of the aerodynamics of spinning and stationary footballs. *Proc IMechE Pt C: J Mech Eng Sci* 222:195–205
- Asai T, Seo K (2013) Aerodynamic drag of modern soccer balls. Springerplus, Berlin
- Murakami M, Kondoh M, Iwai Y, et al. (2010) Measurement of aerodynamic forces and flow field of a soccer ball in a wind tunnel for knuckle effect. In: Sabo A, Litzenberger S, Kafka P, et al. (eds) 8th Conference of the International Sports Engineering Association. Vienna, Austria: Procedia Engineering.
- Hong S, Sakamoto K, Washida Y, et al. (2014) The influence of panel orientation on the aerodynamics of soccer balls. In: James D, Wheat J, Choppin S, et al. (eds) 10th Conference of the International Sports Engineering Association. Sheffield, UK: Procedia Engineering.
- Ward M, Passmore MA, Spencer A et al (2019) Characterisation of football trajectories for assessing flight performance. *Proc Inst Mech Eng P J Sport Eng Technol*. <https://doi.org/10.1177/1754371118774414>. (Epub ahead of print 2019)
- Achenbach E (1972) Experiments on the flow past spheres at very high Reynolds numbers. *J Fluid Mech* 54:565–575
- Achenbach E (1974) The effects of surface roughness and tunnel blockage on the flow past spheres. *J Fluid Mech* 65:113–125
- Choi J, Jeon W-P, Choi H (2006) Mechanism of drag reduction by dimples on a sphere. *Phys Fluids*. <https://doi.org/10.1063/1.2191848>. (Epub ahead of print 2006)
- Won SY, Zhang Q, Ligrani PM (2005) Comparisons of flow structure above dimpled surfaces with different dimple depths in a channel. *Phys Fluids*. <https://doi.org/10.1063/1.1872073>. (Epub ahead of print 2005)
- Acarlar MS, Smith CR (1987) A study of hairpin vortices in a laminar boundary layer. Part 1. Hairpin vortices generated by a hemisphere protuberance. *J Fluid Mech* 175:1–41
- Zhou J, Adrian RJ, Balachandar S et al (1999) Mechanisms for generating coherent packets of hairpin vortices in channel flow. *J Fluid Mech* 387:353–396
- Passmore MA, Rogers D, Tuplin S et al (2012) The aerodynamic performance of a range of FIFA-approved footballs. *Proc IMechE Pt P: J Sports Eng Technol* 226:61–70
- Carré MJ, Goodwill SR, Haake SJ (2005) Understanding the effect of seams on the aerodynamics of an association football. *Proc IMechE Pt C: J Mech Eng Sci* 219:657–666
- Asai T, Seo K, Kobayashi O et al (2007) Fundamental aerodynamics of the soccer ball. *Sports Eng* 10:101–110
- Asai T, Ito S, Seo K, et al. (2012) Characteristics of modern soccer balls. In: Sherwood J, Drane P (eds) 9th Conference of the International Sports Engineering Association. Massachusetts, USA: Procedia Engineering.
- Rogers D (2011) A study of the relationship between surface features and the in-flight performance of footballs. Loughborough University, London
- Hong S, Goff JE, Asai T (2019) Effect of a soccer ball’s surface texture on its aerodynamics and trajectory. *Proc Inst Mech Eng P J Sport Eng Technol*. 233:67–74
- Goff JE, Hong S, Asai T (2020) Influence of surface properties on soccer ball trajectories. In: 13th Conference of the International Sports Engineering Association. Online. pp. 143.
- Passmore MA, Tuplin S, Stawski A (2017) The real-time measurement of football aerodynamic loads under spinning conditions. *Proc IMechE Pt P: J Sports Eng Technol* 231:262–274
- Pasquali A, Schnepf B. (2019) Development of new test methods for the evaluation of aerodynamic performance of footballs. FIFA Report.
- Barber S, Chin SB, Carré MJ (2009) Sports ball aerodynamics: a numerical study of the erratic motion of soccer balls. *Comput Fluids* 38:1091–1100
- IFAB (2020) Laws of the Game 2020 <https://www.theifab.com/documents/?documentType=all&language=en&years=2020> Accessed 14 April 2020
- Johl GS, Passmore MA, Render PM (2004) Design Methodology and Performance of an Indraft Wind Tunnel. *Aeronautical J*. 108:465–473.
- Weisstein EW (2019) Sphere-Sphere Intersection. *Wolfram Alpha*, <http://mathworld.wolfram.com/Sphere-SphereIntersection.html>. Accessed 21 June 2019
- Deserno M (2004) How to generate equidistributed points on the surface of a sphere, https://www.cmu.edu/biolphys/deserno/pdf/sphere_equi.pdf. Accessed 21 June 2019
- University of York (1988) Taguchi L16b Orthogonal Design, <https://www.york.ac.uk/depts/math/tables/l16b.htm>. Accessed 25 October 2019
- HP (2023) HP Multi Jet 3D Printing, <https://www.hp.com/gb-en/printers/3d-printers/products/multi-jet-technology.html>. Accessed 17 February 2023).
- Son K, Choi J, Jeon W-P et al (2011) Mechanism of drag reduction by a surface trip wire on the surface of a sphere. *J Fluid Mech* 672:411–427
- Haake SJ, Goodwill SR, Carré MJ (2007) A new measure of roughness for defining the aerodynamic performance of sports balls. *Proc IMechE Pt C: J Mech Eng Sci* 221:789–806
- Fuss FK (2011) The effect of surface skewness on the super/post-critical coefficient of drag of roughened cylinders. *Procedia Eng* 13:284–289
- Thomas TR (1981) Characterization of surface roughness. *Precis Eng* 3:97–104
- NIST (2003) Engineering statistics handbook, <https://www.itl.nist.gov/div898/handbook/eda/section3/eda35b.htm>. Accessed 12 September 2020

Publisher's Note Springer Nature remains neutral with regard to jurisdictional claims in published maps and institutional affiliations.